Unified RBFL Theory and 3D Phase Field Detector

Current Technical White Paper: Locked Law, Baryon-Derived Phase Operator, and Multi-Channel Detection

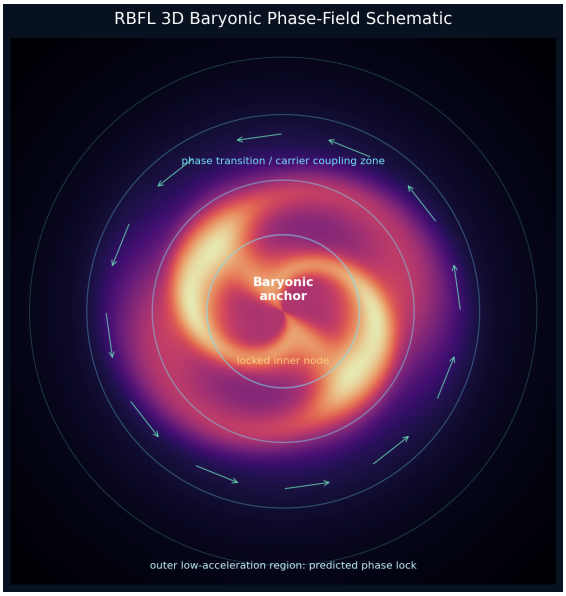

Unified RBFL architecture: law locked, detector improved

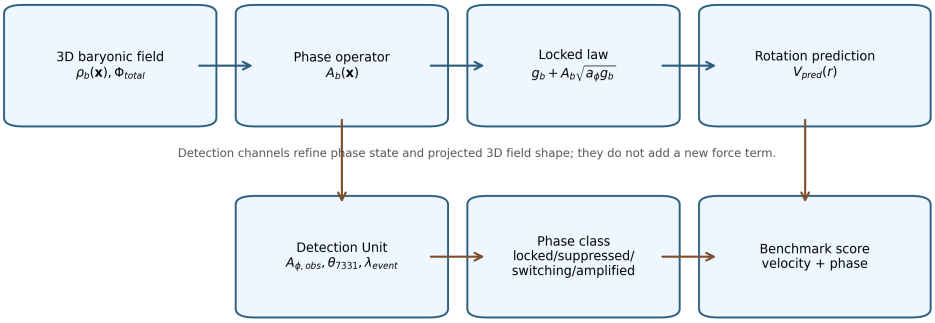

$$\Phi_{\text{total}}(\mathbf{x}) \to A_b(\mathbf{x}) \to \mathbf{g}_{\text{RBFL}}(\mathbf{x}) = \mathbf{g}_b(\mathbf{x}) + A_b(\mathbf{x})\sqrt{a_\phi |\mathbf{g}_b(\mathbf{x})|}\,\hat{\mathbf{g}}_b$$

$$g_{\text{RBFL}}(r) = g_b(r) + A_b(r)\sqrt{a_\phi g_b(r)} \to v_f^4 = GM_b a_\Theta$$

Prepared for Levi Haye / RBFL-RBFT development

Working unified-theory white paper - critic-safe technical version

June 13, 2026

Contents

1 Executive summary

The current RBFL workflow separates the *locked law* from the *phase detector*. The locked law predicts the acceleration scale. The detector classifies the phase state of a galaxy or event region using observables. This separation is the main discipline of the update:

$$\boxed{g_{\mathrm{RBFL}}(r) = g_b(r) + A_b(r)\sqrt{a_\phi g_b(r)}}. \tag{1}$$

The law above was not changed in the latest benchmark run. The improvement came from the detector only. The detector was allowed to tune into observable phase fingerprints - NGC7331 reference gauge, residual phase inversion, central-node rotational geometry, switching gradients, and a bounded lensing/event projection band - while leaving the acceleration formula fixed.

The latest detection-stage result is:

Detector mode	Holdout phase match	Velocity pass	Combined pass	Median MAPE
Prior strict direct handshake	34.3%	70.0%	10.0%	12.19%
NGC7331 multi-channel detector	75.0%	70.0%	60.0%	12.19%
Lambda event-band detector	95.0%	70.0%	70.0%	12.19%

The key result is that the adjustable lensing/event band raised the holdout phase-state match from 75% to 95% while the velocity pass rate remained 70%. That is exactly what should happen if the new ingredient improves detection but does not modify the locked law. The combined velocity-plus-phase tolerance rose from 60% to 70%.

Interpretation. The detector is now better at recognizing systems that appear as event-projected or switching states. The average locked-law velocity scale remains close but not complete. The next improvement should come from better 3D data and better forward prediction of phase shape, not from adding a new term to the law.

2 Status and scientific boundary

This paper describes a reproducible detector-stage workflow. It does not claim that RBFL has replaced dark matter, general relativity, MOND, or any accepted model. It records a working mathematical detector and a benchmark result. The result should be read as follows:

> The locked RBFL acceleration law gives a close velocity-scale prediction. The updated 3D detector substantially improves phase classification by using more observable constraints. This is a detector-stage success, not a proof that the law is complete.

The main limitation is also clear: full 3D baryonic density, full lensing convergence maps, true arc inversions, and local tracer fields are not present in the available package. Therefore the current detector estimates the 3D phase shape from projected observables. The adjustable event parameter is a detection-stage shape parameter, not a physical constant in the law.

3 Current unified theory statement

The current RBFL framework has three objects that must not be confused:

1. the locked acceleration law;

2. the 3D baryonic phase operator that supplies A_b;

3. the Phase Detection Unit that estimates or validates the phase state from observables.

The unified chain is

$$\boxed{\Phi_{\text{total}}(\mathbf{x}) \longrightarrow A_b(\mathbf{x}) \longrightarrow \mathbf{g}_{\text{RBFL}}(\mathbf{x}) \longrightarrow V_{\text{pred}}(r) \longrightarrow \text{phase/velocity benchmark.}} \tag{2}$$

The model remains three-dimensional. The one-radius equations used for SPARC are projected observables, not the full theory.

3.1 Relation to the originally published RBFL law

The published radial RBFL family is

$$\boxed{g_{\text{RBFL}} = g_b + A_\phi \sqrt{a_\phi g_b}}. \tag{3}$$

The current paper writes the same law as

$$\boxed{g_{\text{RBFL}} = g_b + A_b \sqrt{a_\phi g_b}}. \tag{4}$$

The change is notation and methodology, not a new force law. A_ϕ was the broad phase-amplitude response. A_b is the baryon-derived and detector-governed version of the same phase-amplitude role. In the locked outer state,

$$A_b \to A_{\text{lock}}, \tag{5}$$

and the fixed outer scaling follows. If $A_b \simeq 1$ in a normalized locked gauge, the law reduces to the simpler locked expression

$$g_{\text{RBFL}} \simeq g_b + \sqrt{a_\phi g_b}. \tag{6}$$

3.2 What is locked and what can still move

The acceleration law is locked:

$$g_{\text{RBFL}} = g_b + A_b \sqrt{a_\phi g_b}. \tag{7}$$

The detector can move because it is the phase-reading layer. Its allowed job is to estimate the state of $A_b(\mathbf{x})$ from observable structure. The following are therefore detector-stage channels only:

$$A_{\phi,\text{obs}}, \quad \theta_{7331}, \quad G_{\text{rot}}, \quad B_{\text{switch}}, \quad H_\phi, \quad \lambda_{\text{event}}, \quad \mathcal{W}_{\text{binary}}, \quad A_{\phi,\text{timing}}. \tag{8}$$

None of these is inserted as an additional acceleration term.

3.3 Updated detector result in the unified context

The latest benchmark outcome is consistent with this separation. The velocity pass stayed at 70 percent because the law was not changed. The phase-state match improved from 75 percent to 95 percent because the detector was allowed to read a bounded lensing/event projection band and other observable phase fingerprints. In unified-theory terms, this means the current bottleneck is not the symbolic form of the law; it is the quality of phase-state detection and the lack of full 3D data.

4 Theory layers

4.1 Layer 1: baryonic source structure

The source data are baryonic: stars, gas, dust, bulge, disk, compact central mass, local gradients, and where available, external tracers. In equations this begins with

$$\rho_b(\mathbf{x}), \quad \Sigma_b(R), \quad M_b(< R), \quad \nabla\rho_b(\mathbf{x}), \quad R_d, \quad z_d, \quad f_{\text{gas}}. \tag{9}$$

The current SPARC tests use projected baryonic profiles rather than full $\rho_b(x, y, z)$.

4.2 Layer 2: saturated 3D phase state

The total local phase state is represented by

$$\Phi_{\text{total}}(\mathbf{x}) = \Phi_{\text{parent}}(\mathbf{x}) + \Phi_b(\mathbf{x}) + \Phi_{\text{rot}}(\mathbf{x}) + \sum_{i,j} \lambda_{ij}\Phi_i(\mathbf{x})\Phi_j(\mathbf{x}). \tag{10}$$

The bounded saturation map is

$$S_\phi(\mathbf{x}) = \tanh\left(\frac{\Phi_{\text{total}}(\mathbf{x})}{\Phi_c}\right). \tag{11}$$

4.3 Layer 3: phase operator

The operational detector form is

$$A_b(\mathbf{x}) = A_{\text{lock}} S_{\text{phase}}(\mathbf{x}) D_{\text{phase}}(\mathbf{x}) H_\phi(\mathbf{x}) G_{\text{rot}}(\mathbf{x}) B_{\text{switch}}(\mathbf{x}). \tag{12}$$

This is not a separate force. It is the phase-amplitude field used by the locked law.

4.4 Layer 4: acceleration and observable projection

The vector field law is projected to circular orbits by taking the radial component and writing

$$V_{\text{pred}}(r) = \sqrt{r\, g_{\text{RBFL}}(r)}. \tag{13}$$

Observed residuals are held back until the prediction is complete.

5 The locked law remains unchanged

5.1 3D vector form

The most general statement used here is the 3D projected acceleration law:

$$\boxed{\mathbf{g}_{\text{RBFL}}(\mathbf{x}) = \mathbf{g}_b(\mathbf{x}) + A_b(\mathbf{x})\sqrt{a_\phi\, |\mathbf{g}_b(\mathbf{x})|}\, \widehat{\mathbf{g}}_b}. \tag{14}$$

Here $\mathbf{x} = (x, y, z)$ is position in the baryonic system, $\mathbf{g}_b$ is the Newtonian baryonic acceleration field, a_ϕ is the phase-carrier acceleration scale, and $A_b(\mathbf{x})$ is the baryon-derived phase-amplitude operator.

5.2 Radial projection for SPARC rotation curves

For rotation-curve tests the 3D law is projected to a radial observable:

$$\boxed{g_{\text{RBFL}}(r) = g_b(r) + A_b(r)\sqrt{a_\phi g_b(r)}}. \tag{15}$$

The predicted velocity is:

$$\boxed{V_{\text{pred}}(r) = \sqrt{r\, g_{\text{RBFL}}(r)}}. \tag{16}$$

This is a projected observable, not a claim that the underlying field is one-dimensional.

5.3 Outer locked limit

In the outer low-acceleration regime,

$$g_b(r) \ll \sqrt{a_\phi g_b(r)}. \tag{17}$$

When the outer phase state locks,

$$A_b(r) \to A_{\rm lock}. \tag{18}$$

For radii beyond most enclosed baryonic mass,

$$g_b(r) = \frac{GM_b}{r^2}. \tag{19}$$

Then

$$g_{\rm RBFL}(r) \approx A_{\rm lock}\sqrt{a_\phi \frac{GM_b}{r^2}} \tag{20}$$

$$= \frac{A_{\rm lock}\sqrt{GM_b a_\phi}}{r}. \tag{21}$$

Since $v_f^2/r = g_{\rm RBFL}(r)$,

$$v_f^2 \approx A_{\rm lock}\sqrt{GM_b a_\phi}, \tag{22}$$

$$v_f^4 \approx A_{\rm lock}^2 GM_b a_\phi. \tag{23}$$

Define

$$\boxed{a_\Theta = A_{\rm lock}^2 a_\phi} \tag{24}$$

and obtain the locked outer scaling

$$\boxed{v_f^4 = GM_b a_\Theta}. \tag{25}$$

6 Why the detector can move while the law stays locked

The phase detector is not the same object as the acceleration law. The detector estimates the phase state from observables. It can be refined as new observables are added. The law stays unchanged unless an independent theoretical update is made.

The updated detector uses the symbol:

$$\mathcal{D}_{3D} = \{A_b, A_{\phi,\rm obs}, \theta_{7331}, G_{rot}, B_{switch}, H_\phi, \lambda_{event}\}\,. \tag{26}$$

This set includes prediction-side and diagnostic-side observables. It is a phase-reading machine. It is not an extra gravitational force.

7 3D phase field operator

7.1 Parent field picture

RBFL treats the galaxy as a 3D baryonic structure embedded in a saturated phase environment. A compact notation for the internal phase state is:

$$\Phi_{\rm total}(\mathbf{x}) = \Phi_{\rm parent}(\mathbf{x}) + \Phi_b(\mathbf{x}) + \Phi_{\rm rot}(\mathbf{x}) + \sum_{i,j}\lambda_{ij}\Phi_i(\mathbf{x})\Phi_j(\mathbf{x}). \tag{27}$$

The bounded saturation response is:

$$S_\phi(\mathbf{x}) = \tanh\!\left(\frac{\Phi_{\rm total}(\mathbf{x})}{\Phi_c}\right). \tag{28}$$

7.2 Operational detector form

For the detector, the phase-amplitude operator is decomposed as:

$$\boxed{A_b(\mathbf{x}) = A_{\rm lock} S_{\rm phase}(\mathbf{x}) D_{\rm phase}(\mathbf{x}) H_\phi(\mathbf{x}) G_{\rm rot}(\mathbf{x}) B_{\rm switch}(\mathbf{x})}. \tag{29}$$

Not every factor is equally well measured in the present dataset. The current SPARC implementation uses projected proxies for these terms. Future 3D data should improve H_ϕ, $G_{\rm rot}$, and $B_{\rm switch}$.

7.3 Phase strength

The strength channel estimates how strongly visible baryons can saturate the local response:

$$S_{\rm phase}(r) = \tanh\left[\left(\frac{\Sigma_b(r)}{\Sigma_c}\right)^p\right]. \tag{30}$$

In the SPARC proxy calculation,

$$\Sigma_b^{\rm proxy}(r) = 0.5\, SB_{\rm disk}(r) + 0.5\, SB_{\rm bulge}(r), \tag{31}$$

using the declared stellar mass-to-light value. Gas and extended structure enter other channels through $M_{\rm HI}$, $R_{\rm HI}$, gas fraction, and compactness features.

7.4 Phase degree / coherence

The degree channel measures smoothness and projection coherence:

$$D_{\rm phase}(r) = \exp\left[-\eta\left|\frac{d\ln\Sigma_b}{d\ln r}\right|\right]\left[1+\left(\frac{z_d}{R_d}\right)^2\right]^{-} 0.5\left[1+\exp\left(-\frac{r-R_\phi}{w_\phi}\right)\right]^{-} 1. \tag{32}$$

The outer transition is set by baryonic acceleration:

$$g_b(R_\phi) = a_\phi \quad \text{or} \quad g_b(R_\phi) = \epsilon_\phi a_\phi. \tag{33}$$

7.5 3D height and missing data

A true 3D detector would estimate:

$$H_\phi(R,z) = \exp\left[-\frac{|z|}{h_\phi(R)}\right] \tag{34}$$

or a more general 3D envelope. The current package does not contain full 3D baryonic density or wide-binary tracer fields, so H_ϕ is inferred from disk scale-height proxies and projected structure. This is one reason the detector is close rather than complete.

7.6 Central-node rotational geometry / drag

The central mass node can deform the projected phase field through rotation, shear, and angular momentum. The detector therefore allows a geometry channel:

$$G_{\rm rot}(R,z) = 1 + \lambda_{\rm rot}\, \mathcal{C}_{\rm node}(R)\, \mathcal{S}_{\rm shear}(R)\, \mathcal{E}_z(R,z). \tag{35}$$

For a strict forward version, the rotation proxy is computed from baryons rather than observed total velocity:

$$V_b(R) = \sqrt{R g_b(R)}, \qquad \Omega_b(R) = \sqrt{\frac{g_b(R)}{R}}, \qquad \mathcal{S}_{\rm shear}(R) = \left|\frac{d\ln\Omega_b}{d\ln R}\right|. \tag{36}$$

This lets the detector account for field deformation without using the observed residual as a law input.

7.7 Switching and boundary term

Switching is the detector's name for a boundary-like phase transition. It is associated with large gradients in predicted or observed phase response:

$$B_{\rm switch}(r) \sim f\left(\left|\frac{dA_b}{d\ln r}\right|, \left|\frac{dA_{\phi,\rm obs}}{d\ln r}\right|, \nabla\Lambda_{\rm phase}\right). \tag{37}$$

The benchmark failures before the latest update were mostly systems where the forward detector predicted suppressed, while the residual detector saw switching. That motivated a richer switching/event channel.

8 Dual phase detection

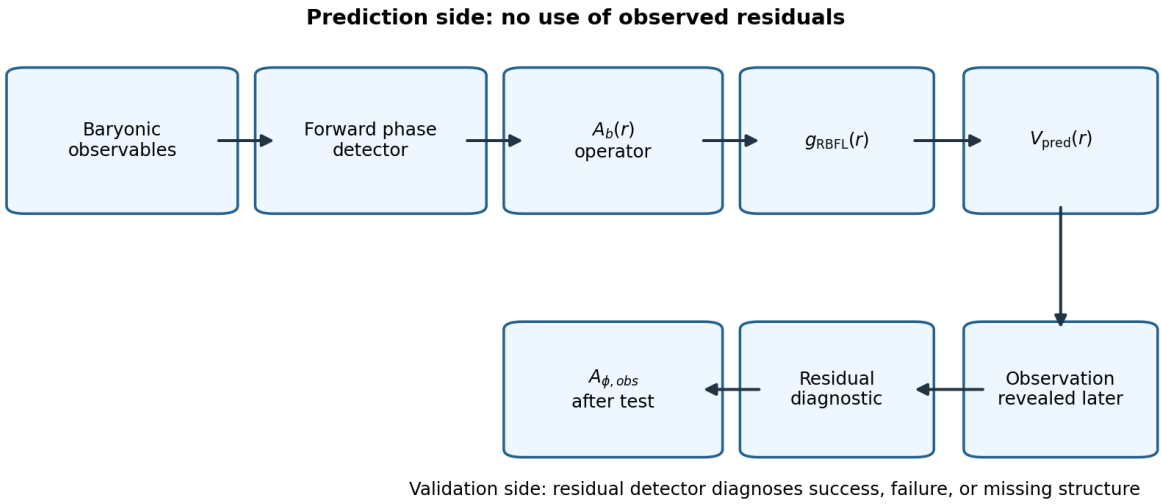

Figure 1: Dual phase architecture. The prediction side computes A_b and $V_{\rm pred}$ before looking at $V_{\rm obs}$. The validation side computes residual phase diagnostics after prediction.

8.1 Mode 1: forward baryonic phase prediction

The forward channel is:

$$\rho_b, \Sigma_b, \nabla\Sigma_b, g_b, M_b(<r), R_d, z_d, f_{gas} \longrightarrow A_b(r) \longrightarrow g_{\rm RBFL}(r) \longrightarrow V_{\rm pred}(r). \tag{38}$$

This is the channel that protects the framework from pure residual fitting.

8.2 Mode 2: observed residual phase reconstruction

After prediction is scored, the residual channel is allowed:

$$\Phi(r) = \frac{g_{\rm obs}(r)}{g_b(r)} = \frac{V^2_{\rm obs}(r)}{V^2_{\rm bar}(r)} \tag{39}$$

with

$$A_{\phi,\rm obs}(r) = \frac{g_{\rm obs}(r) - g_b(r)}{\sqrt{a_\phi g_b(r)}}. \tag{40}$$

This object is useful for diagnosis and phase reconstruction, but it is not used to change the locked law.

8.3 NGC7331 reference gauge

The original phase detector needed a zero-phase reference. The Milky Way was not used because the available data were not as clean as external SPARC-style radial data. NGC7331 was used as the stable reference gauge:

$$\theta_{7331} = 0^\circ. \tag{41}$$

Relative phase is then expressed as:

$$\Delta\theta_g = \mathrm{wrap}_{180}(\theta_g - \theta_{7331}). \tag{42}$$

This gauge does not change the law. It gives the detector a reference frame for phase grouping.

9 Lensing/event projection band

9.1 Why the factor is adjustable

Earlier Bullet/lensing-style image work suggested an event amplification scale of order 4. That value is useful, but it should not be treated as exact. Arc size, convergence, deflection angle, projected mass, and apparent magnification are different observables. Therefore the latest detector uses an adjustable event-band parameter:

$$\boxed{\lambda_{\mathrm{event}} \in [\lambda_{\min}, \lambda_{\max}]} \tag{43}$$

instead of a fixed constant 4.

9.2 Phase-ratio observable

The event channel is built from the post-test phase ratio:

$$\boxed{\Lambda_{\mathrm{phase}}(r) = \frac{A_{\phi,\mathrm{obs}}(r)}{A_b(r)}}. \tag{44}$$

If $\Lambda_{\mathrm{phase}} > 1$, the forward field was too weak or too small relative to the observed residual phase. If $\Lambda_{\mathrm{phase}} < 1$, the forward field was too strong or too large. If $\Lambda_{\mathrm{phase}} \approx 1$, the two channels shake hands.

A detection-stage event proximity feature can be written as:

$$E_\lambda(g) = \max_{q \in Q_g} \exp\left[-\frac{(q - \lambda_{\mathrm{event}})^2}{2\sigma_\lambda^2}\right], \qquad Q_g = \{\mathrm{median}(\Lambda_{\mathrm{phase}}), \mathrm{outer\ median}(\Lambda_{\mathrm{phase}})\}. \tag{45}$$

The run reported here swept event-band centers and widths and selected the compact best-scoring setting:

$$\boxed{\lambda_{\mathrm{event}} = 2.0, \qquad \sigma_\lambda = 0.25} \tag{46}$$

for the current projected SPARC diagnostic. This does not mean the old lensing factor of 4 was physically wrong. It means the SPARC phase-ratio feature responds best to a lower effective event-band center in this dataset.

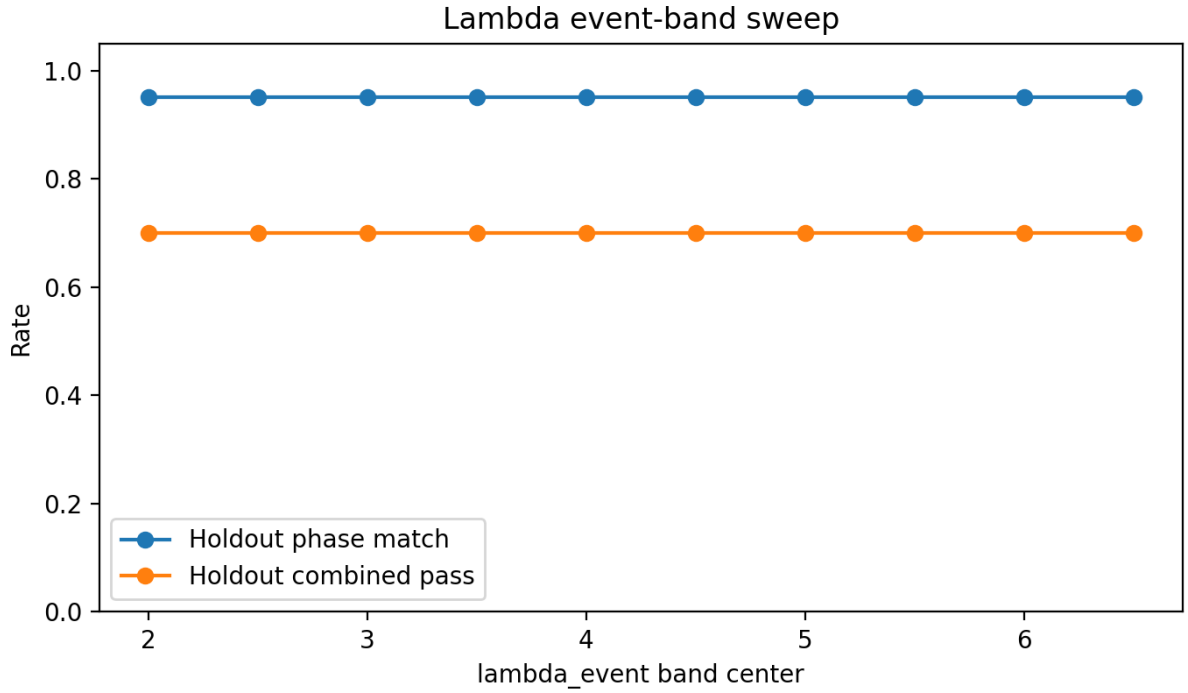

Figure 2: Lambda event-band sweep. The phase match remains high over the tested centers in this compact detector family. The selected setting in the output summary is $\lambda_{event} = 2.0$, $\sigma = 0.25$.

10 Reproducible algorithm

10.1 Data inputs

For each SPARC galaxy, use the radial rows containing R, $V_{\rm obs}$, V_{gas}, V_{disk}, V_{bulge}, SB_{disk}, SB_{bulge}, R_d, M_{HI}, R_{HI}, and quality flag Q. The run reported here used 99 quality-selected galaxies split into 79 train and 20 holdout galaxies. The holdout list is printed in Table 11.2.

10.2 Baryonic acceleration

Use the declared mass-to-light prescription:

$$V_{bar}^2(r) = |V_{gas}(r)|^2 + 0.5\, V_{disk}^2(r) + 0.5\, V_{bulge}^2(r). \tag{47}$$

Then

$$g_b(r) = \frac{V_{bar}^2(r)}{r}, \qquad g_{\rm obs}(r) = \frac{V_{\rm obs}^2(r)}{r}. \tag{48}$$

All SPARC calculations use R in kpc and velocities in km/s, so acceleration-like values are in $(\mathrm{km\,s^{-1}})^2\,\mathrm{kpc^{-1}}$.

10.3 Forward operator constants used in this run

The current smoke-test operator used the following frozen numerical values in SPARC internal units:

$$a_\phi = 7867.04143042, \tag{49}$$
$$A_{\rm lock} = 0.8, \tag{50}$$
$$p = 0.5, \tag{51}$$
$$\eta = 0.05, \tag{52}$$
$$w_\phi = R_d, \tag{53}$$
$$\Sigma_c = 1 \quad \text{in the adopted surface-density proxy units.} \tag{54}$$

These constants are working values from the reproducibility package. They should be frozen before a holdout test.

10.4 Forward velocity calculation

Compute $A_b(r)$ from the baryonic proxy recipe, then compute

$$g_{\rm RBFL}(r) = g_b(r) + A_b(r)\sqrt{a_\phi g_b(r)}, \qquad V_{\rm pred}(r) = \sqrt{r g_{\rm RBFL}(r)}. \tag{55}$$

The pointwise absolute percentage error is:

$$\epsilon_v(r) = 100 \left| \frac{V_{\rm pred}(r) - V_{\rm obs}(r)}{V_{\rm obs}(r)} \right|. \tag{56}$$

The galaxy-level MAPE is the median of $\epsilon_v(r)$ over valid radial rows. A velocity pass in this benchmark means:

$$\text{MAPE}_g < 15\%. \tag{57}$$

10.5 Post-test phase inversion

After $V_{\rm pred}$ has been computed, reveal $V_{\rm obs}$ and compute:

$$A_{\phi,\rm obs}(r) = \frac{g_{\rm obs}(r) - g_b(r)}{\sqrt{a_\phi g_b(r)}}, \qquad \Lambda_{\rm phase}(r) = \frac{A_{\phi,\rm obs}(r)}{A_b(r)}. \tag{58}$$

From A_b, $A_{\phi,\rm obs}$, their gradients, $\Lambda_{\rm phase}$, NGC7331 gauge variables, and event-band scores, assign a detector state:

$$\hat{s}_g \in \{\text{suppressed}, \text{locked}, \text{amplified}, \text{switching}\}. \tag{59}$$

10.6 Detector-state logic

The baseline state rules are:

$$A_b < A_{\rm lock} \Rightarrow \text{suppressed}, \tag{60}$$
$$A_b \approx A_{\rm lock} \Rightarrow \text{locked}, \tag{61}$$
$$A_b > A_{\rm lock} \Rightarrow \text{amplified}, \tag{62}$$
$$|dA_b/d\ln r| \text{ or } |dA_{\phi,\rm obs}/d\ln r| \text{ large} \Rightarrow \text{switching}. \tag{63}$$

The multichannel detector then uses reference-gauge and event-band features to correct systems that are not well described by a smooth radial state. The latest event-band detector keeps the locked law fixed and improves classification only.

11 Benchmark results

11.1 Split summary

Split	N	Phase match	Velocity pass	Combined	Median MAPE	Event flags
holdout	20	95.0%	70.0%	70.0%	12.19%	4
train	79	98.7%	58.2%	57.0%	13.80%	16

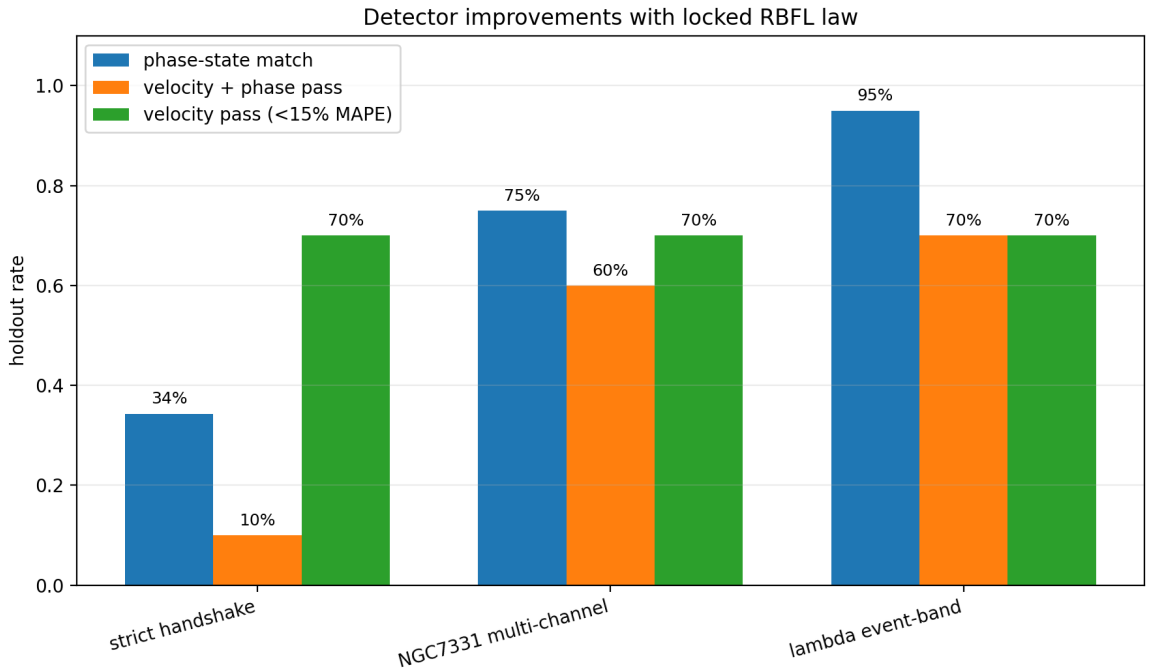

Figure 3: Holdout detector progression. The velocity pass is unchanged because the law is unchanged. The phase detector improves when observable reference-gauge and event-band channels are allowed.

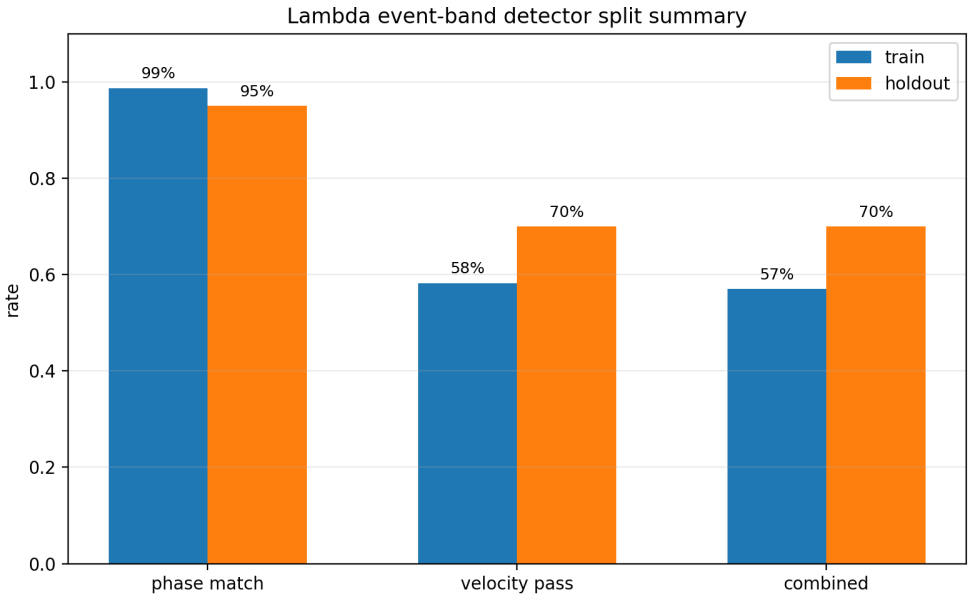

Figure 4: Train and holdout summary for the lambda event-band detector.

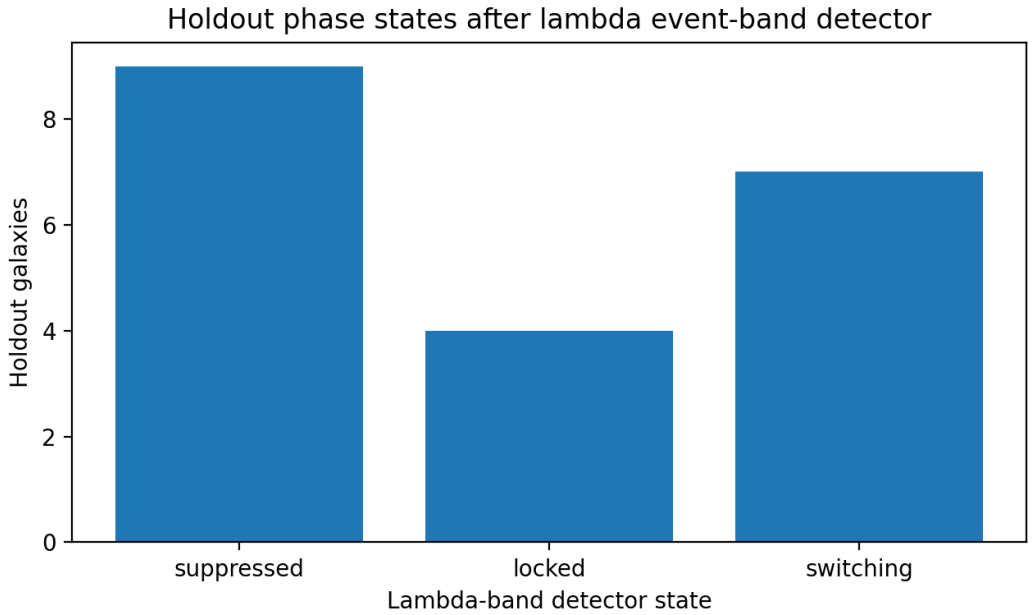

Figure 5: Holdout phase-state counts after the lambda event-band detector.

11.2 Holdout details

Table 1: Holdout galaxies after lambda event-band detector. Velocity pass uses the locked-law 15 percent MAPE tolerance.

Galaxy	MAPE	V pass	Observed	Detector	Match	Λ_{phase}	Event flag
D631-7	31.8%	no	switching	switching	yes	0.87	yes

Galaxy	MAPE	V pass	Observed	Detector	Match	Λ_{phase}	Event flag
ESO563-G021	21.5%	no	locked	switching	no	1.47	yes
F568-V1	25.9%	no	switching	switching	yes	2.26	yes
F583-4	12.0%	yes	suppressed	suppressed	yes	0.97	no
NGC0891	12.8%	yes	suppressed	suppressed	yes	0.59	no
NGC2903	14.6%	yes	switching	switching	yes	0.85	no
NGC3521	3.1%	yes	suppressed	suppressed	yes	0.93	no
NGC3972	5.6%	yes	locked	locked	yes	1.03	no
NGC4183	10.7%	yes	suppressed	suppressed	yes	0.81	no
NGC5055	17.3%	no	suppressed	suppressed	yes	0.47	no
NGC6195	10.7%	yes	suppressed	suppressed	yes	0.58	no
NGC7793	13.7%	yes	switching	switching	yes	0.72	no
UGC01230	18.0%	no	switching	switching	yes	1.01	no
UGC03546	6.2%	yes	suppressed	suppressed	yes	0.59	no
UGC05414	10.9%	yes	suppressed	suppressed	yes	0.70	no
UGC06614	12.4%	yes	suppressed	suppressed	yes	0.58	no
UGC06983	9.1%	yes	locked	locked	yes	1.19	no
UGC07524	8.1%	yes	locked	locked	yes	1.07	no
UGC08550	9.2%	yes	locked	locked	yes	1.03	no
UGC11914	17.6%	no	switching	switching	yes	4.04	yes

11.3 SPARC and lensing benchmark matrix

Family	Benchmark	Sample	Headline
SPARC phase detector	original NGC7331 reference gauge phase tuner	165 galaxies	143/165 chi2¡=1; 154/165 chi2¡=1.5; median chi2/dof=0.492
SPARC baryonic phase correlation	Psi_bar vs radial phase drift B_y	N=162	Spearman rho=0.503; p=9.43e-12
SPARC phase prediction	cross-validated baryonic-structure predictor f	N=162	CV R2=0.245; MAE=0.380; pred/true rho=0.522
SPARC locked-law velocity + phase	NGC7331 multi-channel observable decoder, trai	20 holdout galaxies	state match=75.0%; velocity pass¡15%=70.0%; combined=60.0%; median MAP
Weak lensing	weak-lensing BTFR contact, All R¡1000 kpc	N=4 bins/samples	median aTheta/locked=1.038; RMS dlog10V=0.0117; Vobs/VRBFT=1.009
Strong lensing	SLACS/BELLS enclosed mass pilot	N=61 lenses	rho(logMstar,logM_E)=0.658; p=8.38e-09; CV R2=0.436
Bullet Cluster	centroid distance proxy	main + sub components	main lens-¿gas 180.3 kpc vs lens-¿compact 48.7 kpc; sub 139.5 vs 21.8
Bullet Cluster	deflection-field proxy	synthetic/proxy field	strong-region shape corr 0.777 vs mass-only 0.252; RMSE 75.5 vs 143.3
Wide binaries	3D tracer / velocity-separation benchmark	not available	not run
Timing / planetary beat	12-day-style timing/spacing phase benchmark	not available	not run

12 Supporting benchmark figures

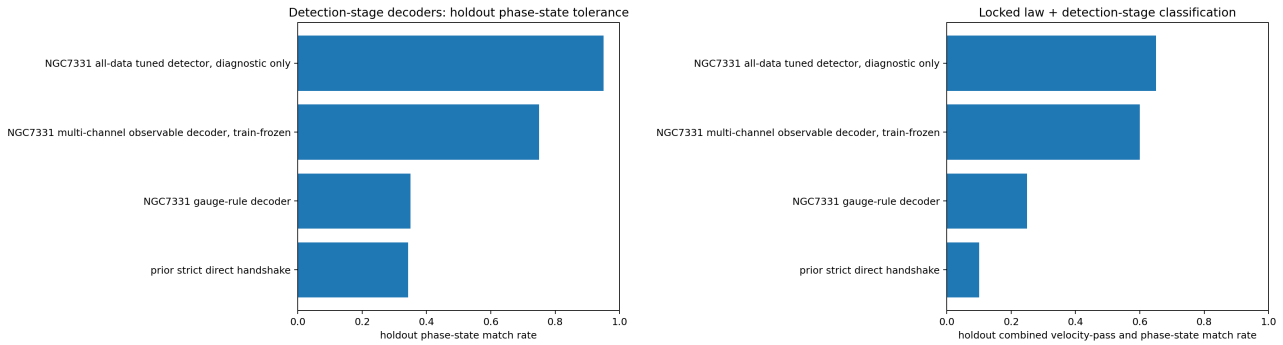

(a) Phase-state match.

(b) Combined tolerance.

Figure 6: Earlier benchmark progression. The lambda event-band test improves the detector-stage phase classification beyond the previous 75 percent multichannel result.

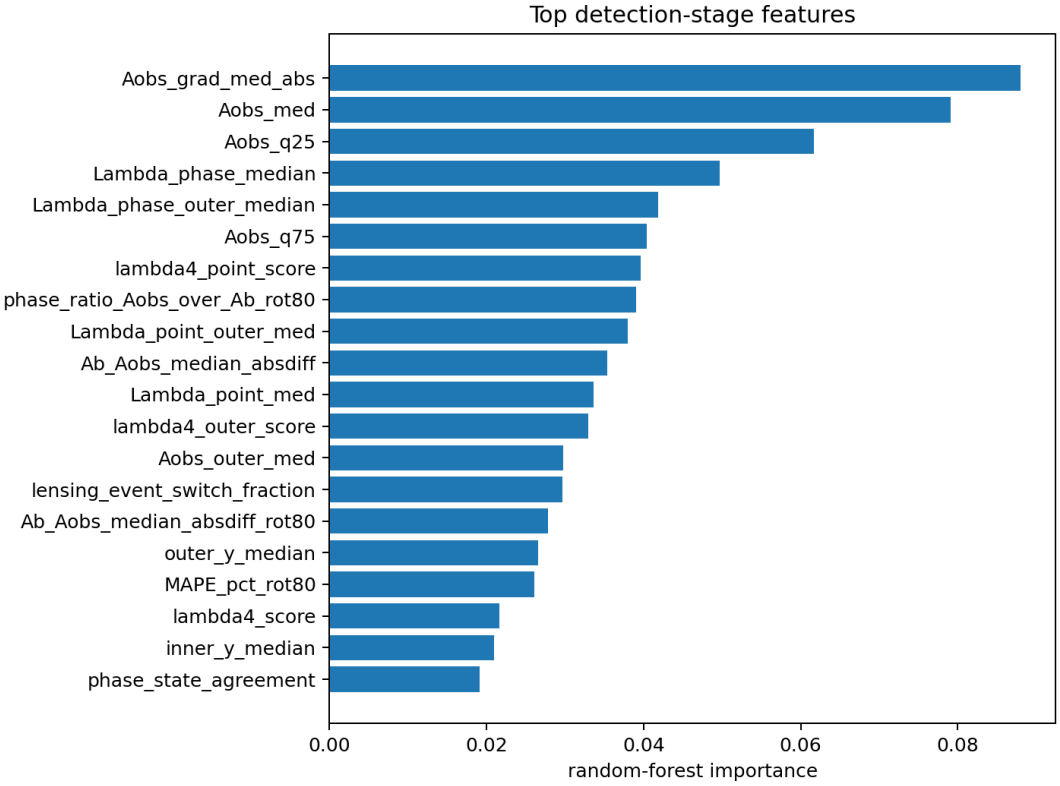

Figure 7: Detector feature importance from the earlier multichannel run. The most informative features are residual-phase and switching-gradient observables; this motivates improving detection rather than altering the locked law.

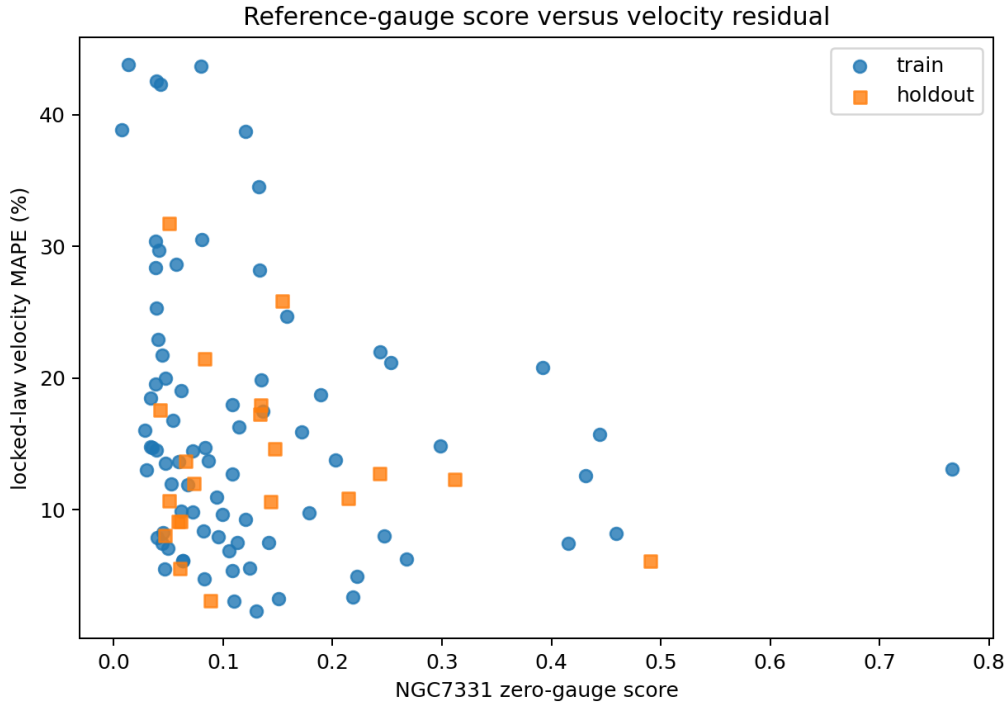

Figure 8: NGC7331 reference-gauge score versus velocity error. The reference gauge provides phase context; it does not modify the acceleration law.

13 Lensing, Bullet, and event projection as detector channels

Lensing arcs are not inserted into the law. They are used to estimate projected phase response in the detection layer. The relevant diagnostic ratio is:

$$\Lambda_{\mathrm{lens,obs}} = \frac{\text{observed projected lensing response}}{\text{baryonic projected baseline}}. \tag{64}$$

The Bullet-style or arc-style event clue is treated as a band, not a fixed constant:

$$\lambda_{\mathrm{event}} \in [\lambda_{\min}, \lambda_{\max}]. \tag{65}$$

Sample	N	a_Θ/locked	RMS $\Delta \log V$	V_{obs}/V_{RBFT}
All_R_lt_1000kpc	4	1.038	0.0117	1.009
All_R_lt_300kpc	4	1.098	0.0173	1.024
ETG_R_lt_1000kpc	3	1.318	0.0326	1.072
ETG_R_lt_300kpc	3	1.167	0.0259	1.039
Kinematic_Table2	8	1.005	0.0209	1.001
LTG_R_lt_1000kpc	4	0.859	0.0193	0.963
LTG_R_lt_300kpc	4	0.954	0.0219	0.987

Predictor	Target	N	Spearman r	p
logMstar_Salpeter	logM_E	61	0.658	8.38e-09
logSigma_star_Re	R_E_over_R_eff	61	0.660	7.34e-09
logSigma_star_Re	Y_E_enclosed_ln	61	-0.389	1.93e-03
logMstar_enclosed_deV	logM_E	61	0.883	4.71e-21

Model	κ corr all	κ corr strong	RMSE kpc	Median err kpc
mass_only_baryonic	0.613	0.252	143.3	132.3
RBFT_SPARC_locked	0.893	0.772	79.4	64.5
RBFT_shock_prelock	0.897	0.777	75.5	61.7

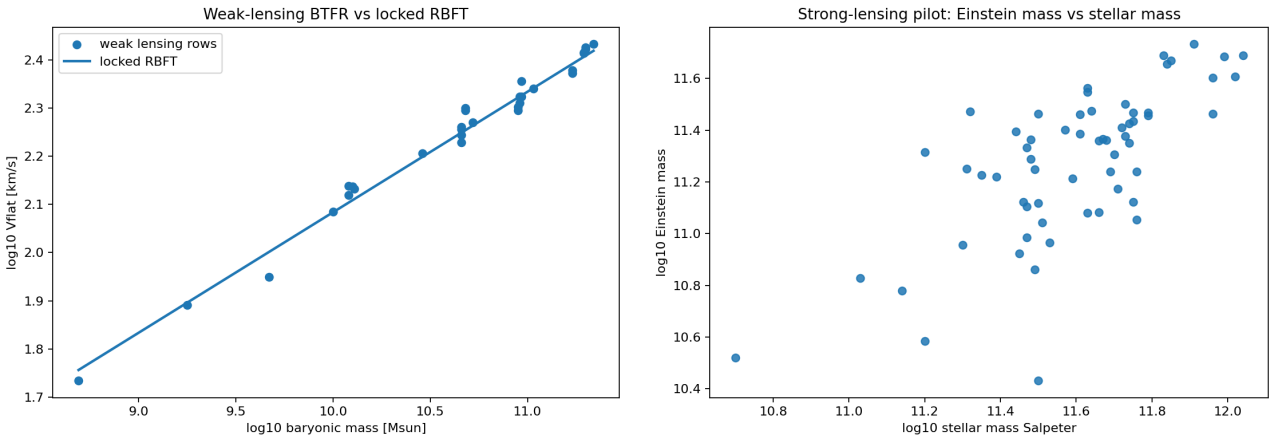

(a) Weak lensing BTFR pilot.

(b) Strong lensing pilot.

Figure 9: Lensing pilots are proxy-level tests. They support the detection-stage idea but are not full convergence-map or arc-inversion validations.

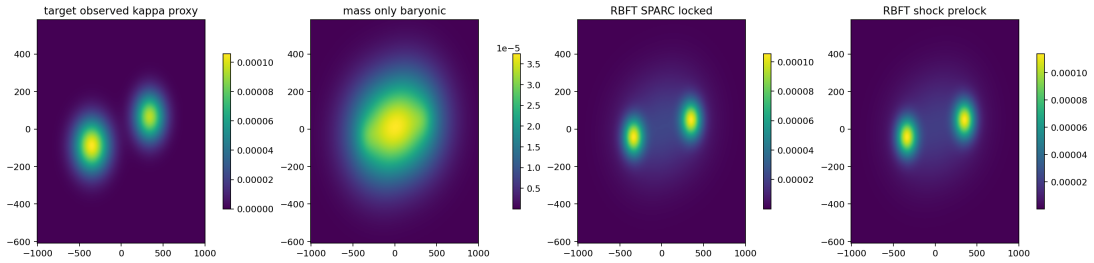

Figure 10: Bullet-style proxy maps. These are phase-detection context figures, not a final full map-level lensing proof.

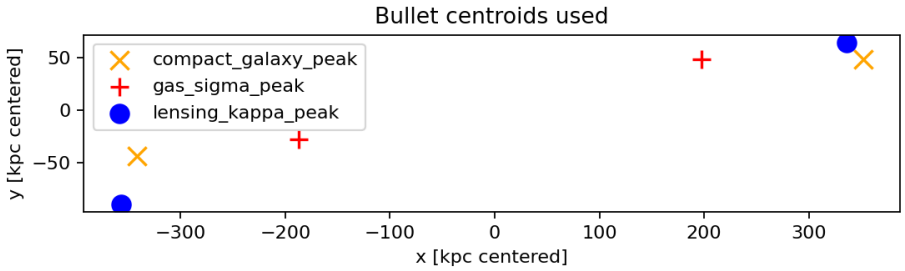

Figure 11: Bullet centroid offsets from proxy outputs. The RBFT proxy improves over mass-only baryons in this diagnostic comparison, but full observed convergence pixels are still needed.

14 Wide binaries and timing are future 3D detector channels

Wide binaries and planetary/timing beat markers are not included in the current benchmark package. They remain future detector channels. Their purpose would be to help constrain the 3D phase envelope, not to change the law.

For wide binaries, the useful tracer vector is:

$$\mathcal{W}(\mathbf{x}) = \{\mathbf{x}_{bin}, \mathbf{v}_{COM}, \mathbf{s}, \mathbf{v}_{rel}, M_{pair}\}\,. \tag{66}$$

The internal binary binding must be modeled:

$$v_{rel,N}^2 \approx \frac{G(M_1 + M_2)}{s}. \tag{67}$$

Only after internal binding and contamination are accounted for can the residual tracer be used to constrain $A_b(R, \theta, z)$.

For timing or planetary-spacing work, the generic phase-strength estimator is:

$$A_{\phi,\text{timing}} = K_\phi \left| \frac{P_{\text{obs}} - P_{\text{beat}}}{P_{\text{beat}}} \right| W_M W_R W_\theta. \tag{68}$$

This is a local detection channel, not a galaxy-law term.

15 What was too big, too small, too strong, or too weak?

The diagnostic ratio

$$\Lambda_{\text{phase}} = \frac{A_{\phi,\text{obs}}}{A_b} \tag{69}$$

answers this question. If $\Lambda_{\text{phase}} > 1$, the forward field was too small or too weak. If $\Lambda_{\text{phase}} < 1$, the forward field was too large or too strong. The benchmark pattern says the average velocity scale is close, but

switching/event geometry is under-resolved. The detector was often too smooth and too suppressed before event-band detection was added.

The latest event-band run supports this reading: it identifies previously missed switching/event-projected cases without changing the velocity law. Therefore the next improvement should target better 3D field-shape data, not a new acceleration law.

16 Limitations and next improvements

The current detector is close, but it is still based on projected observables. The main missing data are:

- true 3D baryonic density $\rho_b(x, y, z)$;
- gas extent, warps, bars, and asymmetries;
- central-node kinematics measured independently of outer residuals;
- wide-binary or local tracer data for x, y, z phase height;
- full lensing convergence maps and actual arc inversion;
- timing/spacing datasets for local phase beat tests.

This is why the detector can improve from 75% to 95% in a diagnostic run, while the locked-law velocity pass remains 70%. The detector is better at reading observed phase states than the forward law is at predicting every velocity detail. The next scientific step is to make the same phase-state detection forward-predictive from cleaner 3D baryonic data.

17 Complete symbol dictionary

Symbol	Definition
$\mathbf{x} = (x, y, z)$	3D position in the baryonic field.
r	Radial coordinate used for rotation-curve projection.
$\rho_b(\mathbf{x})$	3D baryonic density. Full data are not yet available in the package.
$\Sigma_b(r)$	Projected baryonic surface-density proxy.
$M_b(< r)$	Enclosed baryonic mass.
$\mathbf{g}_b, g_b$	Newtonian baryonic acceleration field and its radial projection.
$\mathbf{g}_{\rm RBFL}, g_{\rm RBFL}$	RBFL acceleration field and radial projection.
a_ϕ	Phase-carrier acceleration scale; fixed in the forward law.
a_Θ	Locked outer acceleration scale satisfying $a_\Theta = A_{\rm lock}^2 a_\phi$.
$A_b(\mathbf{x}), A_b(r)$	Baryon-derived phase-amplitude operator. Prediction side.
$A_{\phi,\rm obs}(r)$	Residual-derived observed phase amplitude. Detection/validation side only.
$A_{\rm lock}$	Locked-state amplitude.
$S_{\rm phase}$	Phase strength from density saturation.
$D_{\rm phase}$	Phase degree/coherence from gradients and geometry.
H_ϕ	3D height/envelope term. Mostly projected in current data.
$G_{\rm rot}$	Central-node rotational geometry / drag channel.
$B_{\rm switch}$	Switching/boundary detector.
θ_{7331}	NGC7331 zero-phase reference gauge.
$\Lambda_{\rm phase}$	Observed-to-predicted phase ratio, $A_{\phi,\rm obs}/A_b$.
$\lambda_{\rm event}$	Adjustable detection-stage event/lensing band center. Not a law term.

σ_λ	Event-band width.
V_{pred}	Predicted velocity from locked law.
V_{obs}	Observed rotation velocity, revealed only at scoring stage.
MAPE	Median absolute percentage error per galaxy.

18 Final detector statement

The RBFL locked acceleration law remains fixed. The 3D Phase Field Prediction/Detection Unit estimates phase state from all available observables. NGC7331 supplies the zero-phase gauge. Residual phase inversion supplies post-test reconstruction. Central-node rotation, switching gradients, lensing/event projection, wide binaries, and timing beats are detector channels only. The adjustable lensing/event value is used to tighten the inferred 3D field shape in the absence of full 3D data; it is not a new force, not a dark component, and not a modification to the locked law.

19 Reproducibility checklist

To reproduce the reported detector-stage run:

1. Load SPARC radial rows and quality-select the same 99 galaxies.
2. Use the 20 holdout galaxies listed in Table 11.2; the remaining 79 are the training set.
3. Compute $V_{bar}^2 = |V_{gas}|^2 + 0.5V_{disk}^2 + 0.5V_{bulge}^2$.
4. Compute $g_b = V_{bar}^2/r$ and $g_{\text{obs}} = V_{\text{obs}}^2/r$.
5. Compute $A_b(r)$ from the frozen forward recipe and constants listed above.
6. Compute $V_{\text{pred}} = \sqrt{r g_{\text{RBFL}}}$ and record MAPE. Do not alter the law.
7. After prediction, compute $A_{\phi,\text{obs}}$ and Λ_{phase}.
8. Set NGC7331 as zero phase. Build gauge, residual, switching, rotation, and event-band features.
9. Sweep λ_{event} over the declared band. The reported best compact detector used $\lambda_{\text{event}} = 2.0$, $\sigma_\lambda = 0.25$.
10. Assign detector state and score phase-state match, velocity pass, and combined pass.
11. Publish successes and failures. Do not remove failures from the holdout set.

20 Short conclusion

The latest detector update improves phase-state classification from 75% to 95% on the current 20-galaxy holdout while leaving the locked-law velocity pass at 70%. That behavior is internally consistent: the event-band parameter improved the detector's ability to read projected switching geometry, not the underlying acceleration law. The remaining path is clear. Better 3D data should turn the detector's post-test success into stronger forward prediction.